**ADVANCED
SCIENCE NEWS**
www.advancedsciencenews.com

small
NANO MICRO

Photocatalysis

Thermally Stable Metal-Organic Framework-Templated Synthesis of Hierarchically Porous Metal Sulfides: Enhanced Photocatalytic Hydrogen Production

Juan-Ding Xiao and Hai-Long Jiang*

P*orous nanostructured materials are demonstrated to be very promising in catalysis due to their well accessible active sites. Thermally stable metal-organic frameworks (MOFs) as hard templates are successfully utilized to afford porous metal oxides and subsequently metal sulfides by a nanocasting method. The resultant metal oxides/sulfides show considerable Brunauer–Emmett–Teller (BET) surface areas, by partially inheriting the pore character of MOF templates. Preliminary investigation on the obtained hierarchically porous CdS for water splitting, as a proof of concept, demonstrates its much higher activity than both corresponding bulk and nanosized counterparts, under visible light irradiation. Given the structural diversity and tailorability of MOFs, such synthetic approach may open an avenue to the synthesis of advanced porous materials for functional applications.*

1. Introduction

The depletion of fossil fuel reserves leads to global energy crisis and environmental issue. Hydrogen is an alternative, sustainable and clean energy, and photocatalytic hydrogen production from water splitting has been recognized to be a promising process.[1] Various semiconductors have been developed as photocatalysts for this reaction. Amongst them, cadmium sulfide (CdS) is very promising due to its visible light response (E_g = 2.4 eV) and conduction band placed at a suitable energy level.[2] However, in addition to its propensity to photocorrosion during photocatalytic process, the application of photocatalytic hydrogen production over bulk

CdS suffers from two main drawbacks: the limited active sites on its surface and the fast recombination of photogenerated electrons and holes. To address these issues, the generation of porous nanostructure might be an effective solution to expose more active sites and suppress the electron–hole recombination.[3] Particularly, the photogenerated electrons and holes undergo short transport distance to reach the substrates, and the separation efficiency can be largely accelerated in porous materials, resulting in significant enhancement of photocatalytic activity.

Templating approach is effective to construct porous materials, for which hard (e.g., porous SiO_2) or soft (e.g., surfactant) sacrificial templates were frequently used.[4] Metal-organic frameworks (MOFs), a relatively new class of porous crystalline materials constructed by metal (clusters) and organic linkers exhibit modular assembly, tailorability, ultrahigh surface area, and diverse functionalities.[5] Tremendous efforts have been devoted to the manipulation of the pore sizes and functionality in MOFs for various applications.[6] Recently, some MOFs have been employed as sacrificial templates to prepare porous carbons or other inorganic materials by calcination.[7] Unfortunately, most of MOFs with low thermal stability decompose during the high-temperature treatment, leading to their imperfect "template" role. Therefore, the judicious selection of MOFs with high

J.-D. Xiao, Prof. H.-L. Jiang
Hefei National Laboratory for Physical Sciences at the Microscale
Department of Chemistry
University of Science and Technology of China
Hefei, Anhui 230026, P. R. China
E-mail: jianglab@ustc.edu.cn

The ORCID identification number(s) for the author(s) of this article can be found under https://doi.org/10.1002/smll.201700632.
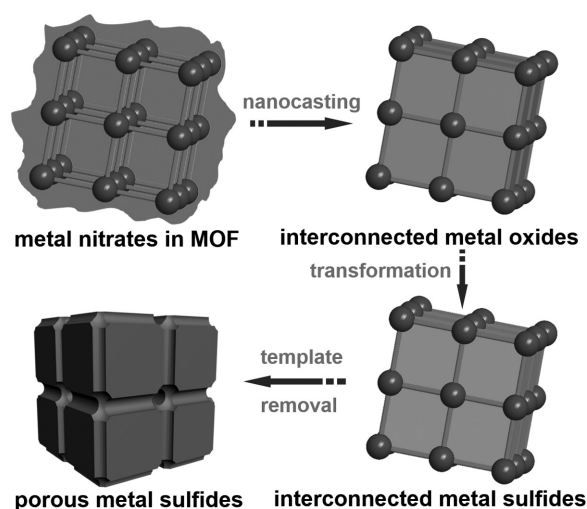
Scheme 1. Schematic illustration for the synthesis of hierarchically porous metal oxides/sulfides templated by MOFs by a nanocasting process.

thermal stability would be necessary to retain their structures during the "nanocasting" process, so that their pore character can be inherited to the duplicate porous materials as far as possible.

Bearing the above considerations in mind, thermally stable MOFs have been chosen as hard porous templates. Several metal nitrates as precursors were incorporated into MOFs to afford metal oxide replica, which can be further converted to metal sulfides within MOFs via a facile sulfuration process. This procedure not only takes advantage of the confinement effect to generate duplicated/inversed pores[8] but also facilitates the template removal skillfully based on the poor chemical stability of MOFs. Upon template removal, the resultant metal oxides/sulfides show considerable Brunauer–Emmett–Teller (BET) surface area, by partially inheriting the pore character of MOF templates (**Scheme 1**). Significantly, as a representative, the hierarchically porous CdS obtained by using MIL-53(Al) template exhibits excellent photocatalytic performance that is superior to the bulk and nanosized CdS counterparts toward hydrogen production by water splitting, manifesting the advantages of the porous nanostructure in photocatalysis.

2. Results and Discussion

2.1. Fabrication of Porous Metal-Oxides Templated by Different MOFs

Three representative 3D MOFs, namely MIL-53(Al) (Al(OH)(BDC), BDC = terephthalic acid), DUT-5 (Al(OH)(bpdc), bpdc = 4,4′-biphenyl dicarboxylate), and ZIF-8 (also called MAF-4, $Zn(MeIM)_2$, MeIM = 2-methylimidazole),[9] featuring considerable BET surface area (Figure S1, Supporting Information) and high thermal stability up to ≈500, 400, and 400 °C, respectively, were deliberately chosen as hard templates. Metal nitrates as metal precursors were incorporated into MOFs via a solvent evaporation approach,[4c] followed by calcination at 350 °C. The $Co(NO_3)_2 \cdot 6H_2O$ was first introduced into MOF templates, MIL-53(Al), DUT-5, and ZIF-8, and the subsequent calcination gave Co_3O_4/MIL-53(Al), Co_3O_4/DUT-5, and Co_3O_4/ZIF-8, respectively. The crystallinity and structure integrity of these MOF templates were maintained to a certain degree during the calcination process, based on the powder X-ray diffraction (XRD) results (Figure S2, Supporting Information). In comparison to thermal stability, the chemical stability of MOFs is mainly determined by the strength of chemical bonding between the inorganic unit and the organic linker, which suggests that MOFs would be easily destroyed in strongly acidic or alkaline solution. Therefore, MIL-53(Al), DUT-5 and ZIF-8 templates were chemically removed by treatment with NaOH, NaOH, and HCl, respectively, to afford hierarchically porous Co_3O_4-1, Co_3O_4-2, and Co_3O_4-3 with high crystallinity (**Figure 1**a).

No characteristic PXRD peaks corresponding to MOF were detected, revealing that the MOF templates have been thoroughly removed. With the peak widths of PXRD, the average crystalline sizes of Co_3O_4-1, Co_3O_4-2, and Co_3O_4-3 were roughly estimated to be 72, 64, and 87 nm, respectively, based on the Scherrer equation.[10] Co_3O_4-1 possesses the highest BET surface area of 234 m^2 g^{-1} compared with the other two samples (114 m^2 g^{-1} for Co_3O_4-2 and 110 m^2 g^{-1} for Co_3O_4-3), which is also higher than most of porous Co_3O_4 samples previously reported (Table S1, Supporting Information), indicating that MIL-53(Al) is the most
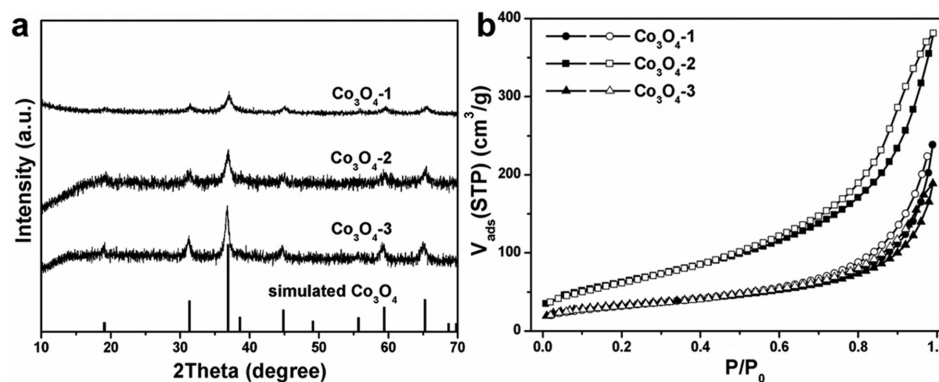
Figure 1. a) Powder XRD profiles and b) N_2 sorption isotherms at 77 K for the as-synthesized Co_3O_4-1, Co_3O_4-2, and Co_3O_4-3 obtained by using MIL-53(Al), DUT-5, and ZIF-8 hard templates, respectively.

promising template in this nanocasting route (Figure 1b). The pore size distribution of Co_3O_4-1 suggests dominative micropores and appears to be the replica of MIL-53(Al) template (Figure S3a,d, Supporting Information), which may be attributed to its highest thermostability and the inherent breathing pore structure.[9a] The mesopore and macropore existed in Co_3O_4-1 possibly arise from the accumulation of MIL-53(Al) particles, and the removal of MIL-53(Al) will leave behind the relatively large pore space. In comparison, the micropores in DUT-5 and ZIF-8 cannot be well inherited, and the dominative mesopores and macropores in Co_3O_4-2 and Co_3O_4-3 should be caused by the lower thermal stability of these two MOFs (Figure S3b,c,e,f, Supporting Information), leading to the collapse of their structures during the calcination. The above observation demonstrates that MIL-53(Al) would be one of the most promising MOF templates suitable for the preparation of hierarchically porous metal oxides via such nanocasting methodology.

To evaluate the universality of MIL-53(Al) template, porous Fe_2O_3 and NiO have also been fabricated using the similar synthetic route. The metal nitrate ($Fe(NO_3)_3·9H_2O$ or $Ni(NO_3)_2·6H_2O$) was introduced into MIL-53(Al), followed by programmed calcination to provide the composite with desired metal oxide penetrated inside the pore structure of MIL-53(Al) (**Figure 2**a). Upon the removal of the template, hierarchically porous Fe_2O_3-1 and NiO-1 with BET surface areas of 430 and 295 m^2 g^{-1}, respectively, were successfully produced with similar micropores as that in MIL-53(Al) (Figure 2b–d). The hierarchically porous structures of Fe_2O_3-1, Co_3O_4-1, and NiO-1 obtained based on MIL-53(Al)

template were further characterized by transmission electron microscopy (TEM) (Figure S4a–c, Supporting Information), where the highly porous structure from continuously connected MOF networks was clearly observable. The successful fabrication of the hierarchically porous Fe_2O_3-1, Co_3O_4-1, and NiO-1 with high BET surface areas and continuous pores unambiguously manifest the superiority of MIL-53(Al) as a hard template. In sharp contrast, powder XRD profiles and N_2 sorption isotherms reveal that direct calcination of $Fe(NO_3)_3·9H_2O$, $Co(NO_3)_2·6H_2O$, and $Ni(NO_3)_2·6H_2O$ under identical conditions except for the absence of MOF templates results in Fe_2O_3, Co_3O_4, and NiO with very low BET surface areas of 89, 43, and 6.7 m^2 g^{-1}, respectively, and broad pore size distributions (Figures S5 and S6, Supporting Information), again highlighting the advantage of MIL-53(Al) template.

2.2. Fabrication of Porous Metal-Sulfides Templated by MIL-53(Al)

The obtained porous metal oxides/MOF composites can be further transformed to other functional porous composites by a facile process. Given that metal chalcogenides, particularly CdS, are promising in photocatalysis,[2b–f] hierarchically porous CdS (denoted as HP-CdS) was fabricated by using MIL-53(Al) as a hard template. Typically, CdO/MIL-53(Al) composite was first fabricated following the above approach (Figure S7, Supporting Information), subsequently introducing Na_2S dropwise to realize the "oxide-to-sulfide" transformation at low temperature. Finally, MIL-53(Al)
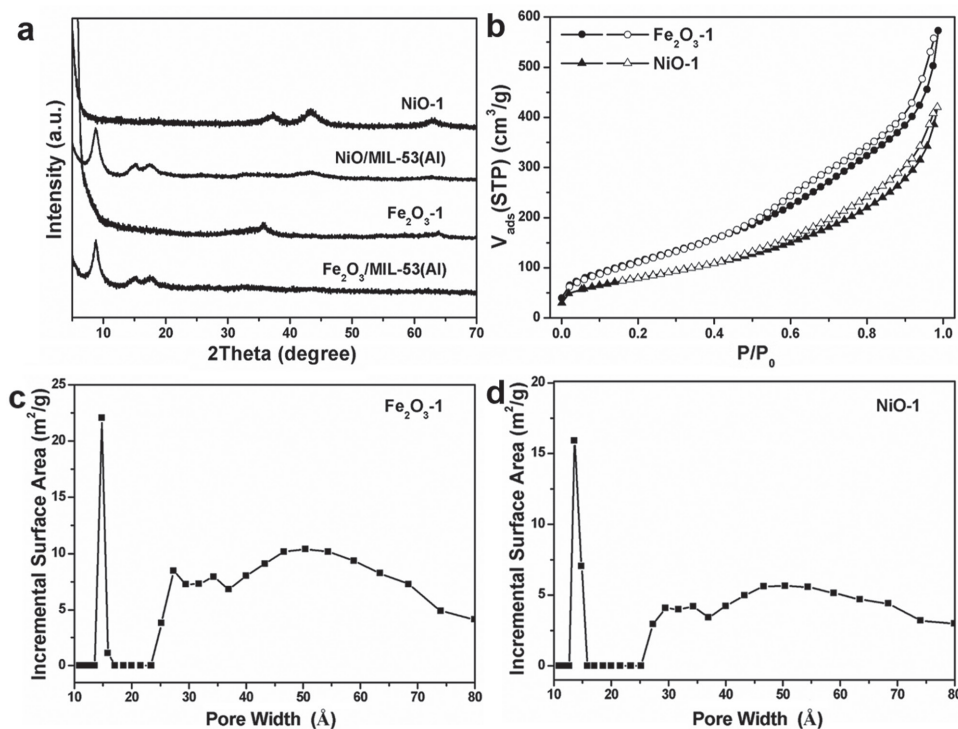
Figure 2. a) Powder XRD profiles for Fe_2O_3-1 and NiO-1 before and after removing MIL-53(Al) template. b) N_2 sorption isotherms at 77 K, and pore size distributions based on density functional theory (DFT) calculation method for c) Fe_2O_3-1 and d) NiO-1 templated by MIL-53(Al). The BET surface areas are 430 and 295 m^2 g^{-1}, corresponding to Fe_2O_3-1 and NiO-1, respectively.
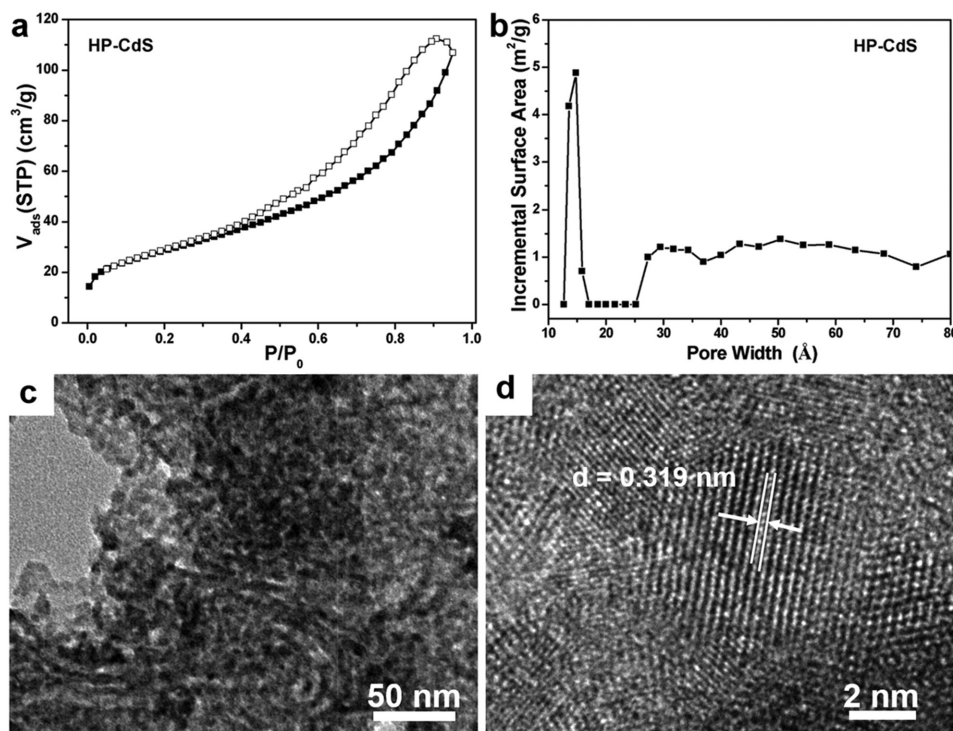
Figure 3. a) N_2 sorption isotherms at 77 K. b) The corresponding pore size distribution based on DFT method. c) TEM and d) HRTEM images for the as-synthesized HP-CdS obtained by using MIL-53(Al) hard template.

template was removed to afford HP-CdS with BET surface area of 119 m^2 g^{-1} and its micropore size is similar to that in MIL-53(Al) as well (**Figure 3**a,b), indicating the favorable template role of the MOF. The average crystalline size of HP-CdS was roughly evaluated to be 58 nm by Scherrer equation based on PXRD peak width,[10] which was further supported by scanning electron microscopy (SEM) observation (Figure S8, Supporting Information). The porous structure of HP-CdS was also proved by TEM observation, presenting the pores distributed throughout the structure (Figure 3c). The high-resolution TEM (HRTEM) image in Figure 3d gives additional evidence for the crystalline CdS, in which the measured lattice spacing of 0.319 nm corresponds to the (101) plane of CdS. In fact, the same procedure can also be adopted to offer other photoactive metal chalcogenides. As another representative, hierarchically porous CuS-1 has been obtained as well based on MIL-53(Al) template (Figures S4d, S9, and S10, Supporting Information), indicating the universality of this synthetic methodology to a certain degree.

2.3. Optical and Electrochemical Measurements

Given that porous photocatalysts are very attractive as the porous structures facilitate the exposure of more active sites and fast charge separation, as well as mass transfer,[3d,e] the porous structure of CdS is expected to greatly improve the charge separation and photocatalytic performance. For comparison, bulk CdS was purchased and nanosized CdS (denoted as nano CdS) was synthesized according to the

reported method (Figures S11 and S12, Supporting Information),[11] to evaluate the superiority of HP-CdS.

UV–vis spectra for bulk CdS, nano CdS, and HP-CdS indicate their comparable light absorption in the region of ≈300–650 nm and roughly similar bandgaps (**Figure 4**a). The photoluminescence (PL) emission spectroscopy can give information for photoexcited charge transfer and recombination processes. As can be seen from Figure 4b, the PL intensity of HP-CdS gets greatly weakened compared with the bulk or nano CdS counterparts. This observation indicates that the photogenerated electron–hole recombination is more efficiently suppressed in HP-CdS. Photocurrent measurements have also been carried out to unveil the charge-separation efficiency. The results show that the photocurrent for HP-CdS gets remarkably enhanced compared to bulk and nano CdS, suggesting the best separation efficiency of photogenerated electron–hole pairs in HP-CdS (Figure 4c). This conclusion is further supported by the electrochemical impedance spectroscopy (EIS) results (Figure 4d), in which HP-CdS exhibits the smallest radius, revealing the lowest charge-transfer resistance. The distinctly different photoelectrochemical properties of HP-CdS from the bulk and nano CdS infer that the HP-CdS would possess much enhanced photocatalytic activity.

2.4. Photocatalytic Hydrogen Production by Water Splitting

Encouraged by these characterization results, we intend to investigate the photocatalytic performance of different forms of CdS in the hydrogen production by water splitting.
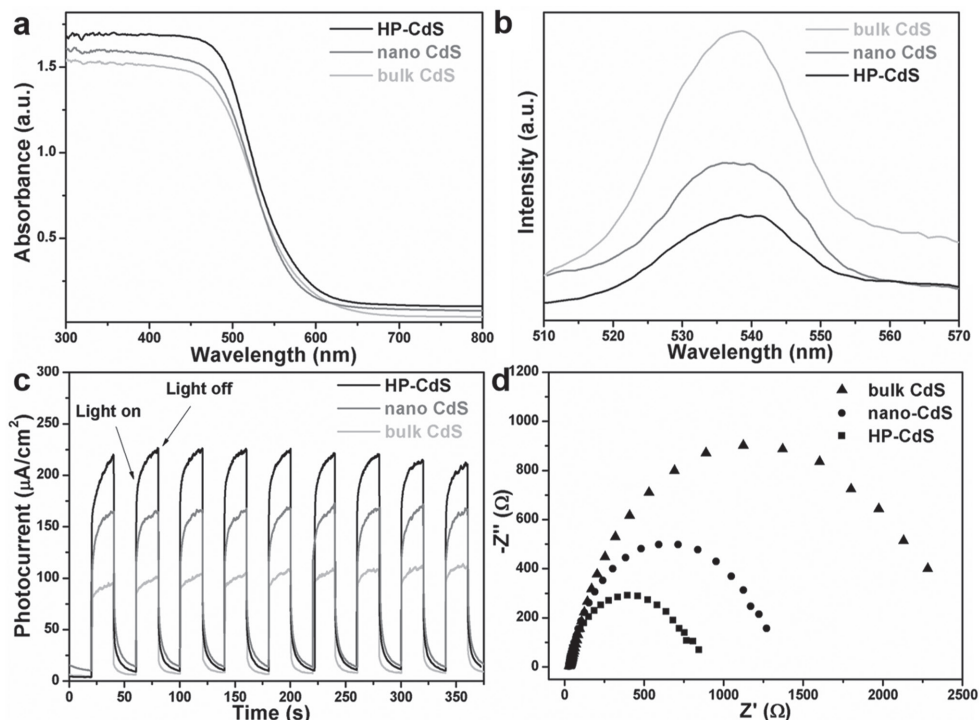
Figure 4. a) UV–vis diffuse reflectance spectra, b) photoluminescence emission spectra, c) photocurrent response, and d) EIS Nyquist plots for the bulk CdS, nano CdS as well as HP-CdS templated by MIL-53(Al).

The photocatalytic hydrogen production was conducted in Na_2S/Na_2SO_3 aqueous solution under visible light irradiation. Compared to the poor activity (115.4 µmol g^{-1} h^{-1}) of bulk CdS, nano CdS exhibits a relatively higher photocatalytic efficiency (350.1 µmol g^{-1} h^{-1}) (**Figure 5**a), which can be attributed to enhanced light absorption, larger specific surface area, and more exposed active sites in nano CdS with improved charge transfer and separation properties, thanks to quantum size effect in nanostructured photocatalysts.[12] Remarkably, the HP-CdS exhibits a significantly enhanced activity (634.0 µmol g^{-1} h^{-1}), which is ≈2 and 5 times higher than that of nano CdS and bulk CdS, respectively. The superior photocatalytic efficiency of HP-CdS should be ascribed to the nanosize effect and porous structure (Figure 3; Figure S8, Supporting Information). Further experiments for HP-CdS

demonstrate that no obvious change occurs to hydrogen production rate during the four catalytic runs (Figure 5b), indicating its excellent catalytic recyclability. The crystallinity and structural integrity of HP-CdS are well retained based on the PXRD profiles and N_2 sorption data (Figures S13 and S14, Supporting Information).

The above results clearly suggest that, the inherent porous structure and large surface area of catalyst have crucial influence on photocatalytic performance of hydrogen production. The tentative photocatalytic mechanism over HP-CdS is proposed as the following. Under visible light irradiation, the excited electrons transfer to the surface of CdS clusters, subsequently react with the adsorbed proton to produce hydrogen. In the case of nano or bulk CdS, most of the photogenerated electrons will be trapped in the interior
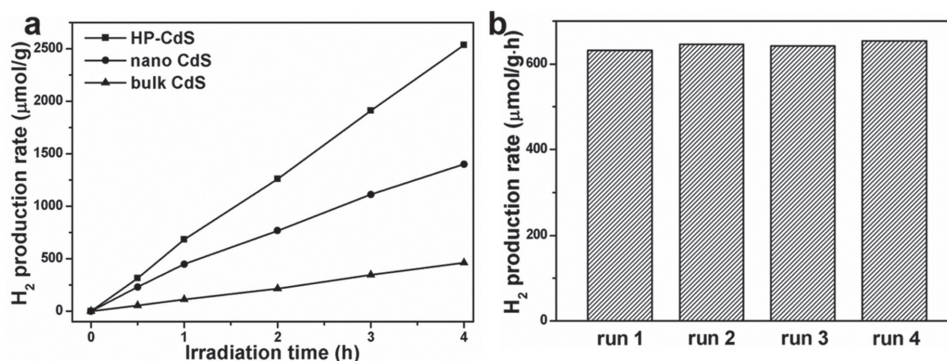
Figure 5. a) Comparison of the photocatalytic hydrogen production rates of the bulk CdS, nano CdS, and HP-CdS. b) Catalytic recyclability of HP-CdS in the hydrogen production by water splitting. The reaction with each photocatalyst (10 mg) in the Na_2S/Na_2SO_3 (0.1 M, 20 mL) aqueous solution is irradiated by light in the spectral region of 380–800 nm.

and recombine with holes due to the lack of sufficient active sites and proton transfer channels, which, however, can be effectively avoided in HP-CdS. The photogenerated electrons can quickly transport to reach the protons, which thoroughly dispersed into the channels of HP-CdS (Scheme S1, Supporting Information), thus resulting in efficient electron–hole separation to realize high activity of hydrogen production.

3. Conclusion

In summary, we have rationally fabricated hierarchically porous metal oxides and sulfides based on thermally stable MOFs as hard templates. The MOF, MIL-53(Al), remains intact during the high-temperature calcinations to afford metal oxides and sulfides. Upon MOF template removal, the replica of porous metal oxides/sulfides can be successfully obtained. As a representative, the as-synthesized HP-CdS possesses remarkably higher photocatalytic hydrogen production activity than the corresponding bulk or nanosized counterparts, due to effective inhibition of electron–hole recombination, thanks to the nanosize effect and porosity in HP-CdS catalyst. Given the huge diversity and high tailorability of MOFs, a variety of MOF-templated metal oxides/sulfides with adjustable pore character and enhanced properties might be achieved. The approach reported in this work would open a new avenue to the development of novel porous functional materials for a broad scope of applications.

4. Experimental Section

Materials and Instrumentation: All chemicals were obtained from commercial sources and used without further purification. Powder X-ray diffraction patterns were obtained on a Holland X'Pert PRO fixed anode X-ray diffractometer equipped with graphite-monochromated Cu Kα radiation ($\lambda = 1.54178$ Å). The nitrogen sorption isotherms were measured by using automatic volumetric adsorption equipment (Micrometritics ASAP 2020). UV–vis diffuse reflectance data were recorded in a Shimadzu Solid Spec-3700 spectrophotometer in the wavelength range of 200–800 nm. Steady-state PL emission spectra were obtained over an LS-55 fluorescence spectrometer made by PerkinElmer. Field-emission SEM was carried out with a field emission scanning electron microanalyzer (Zeiss Supra 40 scanning electron microscope at an acceleration voltage of 5 kV). The size, morphology, and microstructure were investigated by using TEM on JEOL-2010 instruments. The catalytic reaction products were analyzed and identified by gas chromatography (GC, Shimadzu GC-2014).

Synthesis of ZIF-8: Typically, zinc nitrate tetrahydrate (0.210 g, 0.8 mmol) and 2-methylimidazole (0.060 g, 0.73 mmol) were mixed and dissolved in 18 mL N,N-dimethylmethanamide (DMF) in a 20 mL glass vial. The vial was capped and heated to 140 °C for 24 h. After cooling down to room temperature, the product was collected by centrifugation and washed with DMF (5 mL × 3) and methanol (5 mL × 3), finally dried in a vacuum oven overnight.

Synthesis of DUT-5: Typically, 4,4′-biphenyldicarboxylic acid (0.104 g, 0.43 mmol) was dissolved in 10 mL DMF, then Al(NO$_3$)$_3$·9H$_2$O (0.208 g, 0.56 mmol) was added and the mixture was charged into a 100 mL Teflon-lined bomb to react at 120 °C for 24 h. After cooling down to room temperature, the product was collected by centrifugation, and washed with DMF (5 mL × 3) and methanol (5 mL × 3), finally dried in a vacuum oven overnight.

Synthesis of MIL-53(Al): Typically, Al(NO$_3$)$_3$·9H$_2$O (1.5 mmol), H$_2$BDC (1.0 mmol), and P123 (Ma = 5800, 0.3 mmol) were dissolved in a mixed solvent of DMF (7.5 mL), H$_2$O (2.75 mL), and C$_2$H$_5$OH (2.0 mL) under stirring. This clear gel was continuously stirred for 2 h and then charged into a 20 mL Teflon-lined bomb to react at 145 °C for 24 h. The white powder was obtained by filtration, and washed with deionized H$_2$O and C$_2$H$_5$OH for several times, finally dried in a vacuum oven overnight.

Synthesis of Porous Metal Oxides by Using MOF Templates: Typically, Fe(NO$_3$)$_3$·9H$_2$O or Co(NO$_3$)$_2$·6H$_2$O or Ni(NO$_3$)$_2$·6H$_2$O (0.5 g) was dissolved in C$_2$H$_5$OH (40 mL), followed by the addition of MOF (0.5 g). Then, the mixture was stirred at room temperature until all solvent was evaporated off in a fume hood. The powder was collected and redispersed in dry *n*-hexane (20 mL) under stirring in a beaker. When all solvent was evaporated off, the sample was then heated slowly to 350 °C and pyrolyzed at the temperature for 6 h. The resultant sample was treated twice with NaOH (2 M) or HCl (1 M) to remove the MOF, followed by washing with H$_2$O and C$_2$H$_5$OH for several times and then drying at 60 °C under vacuum, finally the porous Fe$_2$O$_3$, Co$_3$O$_4$ or NiO replica can be harvested. Yields based on metal nitrates: Fe$_2$O$_3$-1 (0.062 g, 62.8%), Co$_3$O$_4$-1 (0.090 g, 65.3%), NiO-1 (0.056 g, 43.8%), Co$_3$O$_4$-2 (0.082 g, 59.5%), Co$_3$O$_4$-3 (0.071 g, 51.4%).

Synthesis of Porous Metal Sulfides by Using MOF Templates: Typically, Cd(NO$_3$)$_2$·4H$_2$O or Cu(NO$_3$)$_2$·3H$_2$O (0.5 g) was dispersed in C$_2$H$_5$OH (40 mL), followed by the addition of the MOF (0.5 g). Then, the mixture was stirred at room temperature until all solvent was evaporated off in a fume hood. The powder was collected and redispersed in dry *n*-hexane (20 mL) under stirring in a beaker. When all solvent was evaporated off, the sample was then heated slowly to 350 °C and pyrolyzed at that temperature for 6 h. The resultant sample was redispersed in CH$_3$OH (20 mL) at 60 °C, followed by dropwise adding Na$_2$S (2 mmol), and kept stirring for 12 h, to produce CdS or CuS. The product was collected by centrifugation, and treated twice with NaOH (2 M) to destroy the MOF template, followed by washing with H$_2$O and CH$_3$OH for several times to remove the excess NaOH and residual Al and organic species, and then drying at 60 °C under vacuum, finally the hierarchically porous CdS or CuS can be obtained. Yields based on metal nitrates: HP-CdS (0.106 g, 45.3%), HP-CuS (0.083 g, 41.9%).

Synthesis of Nano CdS: The synthesis of nano CdS was based on previous reports with modifications.[11] Typically, a 50 mL round-bottom flask with 10 mL CH$_3$OH was heated to reach 60 °C. To obtain CdS nanoparticles, 5 mL of Cd(CH$_3$COO)$_2$ (0.4 M) methanolic solution and 5 mL of Na$_2$S (0.4 M) methanolic solution were simultaneously added into the flask in a drop-by-drop way, under vigorous stirring. The resultant yellow mixture was kept stirring for an additional 1 h. Product was collected by centrifugation and washed with H$_2$O/CH$_3$OH mixture. The obtained wet solids were further hydrothermally treated in 60 mL pure water in Teflon-lined stainless steel autoclave (100 mL) at 200 °C for 3 d. The final

yellow product was filtered and washed with H_2O and CH_3OH for several times, and eventually dried in a vacuum overnight.

Photoelectrochemical Measurements: Photocurrent measurements were performed on a CHI 760E electrochemical work station (Chenhua Instrument, Shanghai, China) in a standard three-electrode system with the photocatalyst-coated indium tin oxide (ITO) as the working electrode, Pt plate as the counter electrode, and an Ag/AgCl as a reference electrode. A 0.1 M Na_2SO_3 and 0.1 M Na_2S aqueous solution was used as the electrolyte. The as-synthesized sample (5 mg) was added into 10 µL Nafion and 1.5 mL ethanol mixed solution, and the working electrode was prepared by dropping the suspension (200 µL) onto the surface of an ITO plate. The working electrode was dried at room temperature, and the photoresponsive signals of the samples were measured under chopped light.

The electrochemical impedance spectroscopy was performed on the Zahner Zennium electrochemical workstation in a standard three-electrode system with the photocatalyst-coated glassy carbon ($\Phi = 3$ cm) as the working electrode, Pt plate as the counter electrode, and an Ag/AgCl as a reference electrode. A 0.1 M Na_2SO_3 and 0.1 M Na_2S aqueous solution was used as the electrolyte. The as-synthesized sample (5 mg) was added into 10 µL Nafion and 1.5 mL ethanol mixed solution, and the working electrode was prepared by dropping the suspension (20 µL) onto the surface of the glassy carbon electrode. The working electrode was dried at room temperature, and then EIS measurement was performed with a bias potential of 0.4 V in the dark with a frequency range from 10^{-2} to 10^5 Hz in nitrogen atmosphere.

Photocatalytic Hydrogen Production: The photocatalytic hydrogen production experiments were carried out in a 100 mL optical reaction vessel with stirring at ambient temperature using a 300 W Xe lamp equipped with a UV cutoff filter (>380 nm). Typically, the photocatalyst (10 mg) was dispersed in 20 mL Na_2S (0.1 M) and Na_2SO_3 (0.1 M) aqueous solution, and then the suspension was stirred and purged with nitrogen for ≈40 min to remove air. The reaction vessel filled with the reacting solution was irradiated by the Xe lamp. Hydrogen was measured by gas chromatography (Shimadzu GC-2014, nitrogen as a carrier gas) using a thermal conductivity detector. For each evaluation of hydrogen generation, 200 µL of the headspace was injected into the GC and was quantified by a calibration plot to the internal hydrogen standard.

Supporting Information

Supporting Information is available from the Wiley Online Library or from the author.

Acknowledgements

Conflict of Interest

The authors declare no conflict of interest.

[1] a) Z. Zou, J. Ye, K. Sayama, H. Arakawa, *Nature* **2001**, *414*, 625; b) A. J. Esin, D. G. Nocera, *Chem. Rev.* **2007**, *107*, 4022; c) A. Kudo, Y. Miseki, *Chem. Soc. Rev.* **2009**, *38*, 253; d) X. Wang, K. Maeda, A. Thomas, K. Takanabe, G. Xin, J. M. Carlsson, K. Domen, M. Antonietti, *Nat. Mater.* **2009**, *8*, 76; e) A. Dhakshinamoorthy, A. M. Asiri, H. García, *Angew. Chem. Int. Ed.* **2016**, *55*, 5414.

[2] a) L. Shen, S. Liang, W. Wu, R. Liang, L. Wu, *J. Mater. Chem. A* **2013**, *1*, 11473; b) K. Wu, Z. Chen, H. Lv, H. Zhu, C. L. Hill, T. Lian, *J. Am. Chem. Soc.* **2014**, *136*, 7708; c) S. Saha, G. Das, J. Thote, R. Banerjee, *J. Am. Chem. Soc.* **2014**, *136*, 14845; d) K. A. Brown, M. B. Wilker, M. Boehm, G. Dukovic, P. W. King, *J. Am. Chem. Soc.* **2012**, *134*, 5627; e) L. J. Zhang, S. Li, B. K. Liu, D. J. Wang, T. F. Xie, *ACS Catal.* **2014**, *4*, 3724; f) R. Lin, L. Shen, Z. Ren, W. Wu, Y. Tan, H. Fu, J. Zhang, L. Wu, *Chem. Commun.* **2014**, *50*, 8533.

[3] a) J.-L. Wang, C. Wang, W. Lin, *ACS Catal.* **2012**, *2*, 2630; b) Q. Xiang, B. Cheng, J. Yu, *Appl. Catal. B: Environ.* **2013**, *138–139*, 299; c) W. Zhou, W. Li, J.-Q. Wang, Y. Qu, Y. Yang, Y. Xie, K. Zhang, L. Wang, H. Fu, D. Zhao, *J. Am. Chem. Soc.* **2014**, *136*, 9280; d) V. S. Vyas, F. Haase, L. Stegbauer, G. Savasci, F. Podjaski, C. Ochsenfeld, B. V. Lotsch, *Nat. Commun.* **2015**, *6*, 8508; e) Q. Lin, X. Bu, C. Mao, X. Zhao, K. Sasan, P. Feng, *J. Am. Chem. Soc.* **2015**, *137*, 6184.

[4] a) L. Yu, H. Hu, H. B. Wu, X. W. Lou, *Adv. Mater.* **2017**, *29*, 1604563; b) Y. Shi, Y. Wan, D. Zhao, *Chem. Soc. Rev.* **2011**, *40*, 3854; c) B. T. Yonemoto, G. S. Hutchings, F. Jiao, *J. Am. Chem. Soc.* **2014**, *136*, 8895; d) Z. Yang, Y. Zhang, Z. Schnepp, *J. Mater. Chem. A* **2015**, *3*, 14081.

[5] a) H.-C. Zhou, J. R. Long, O. M. Yaghi, *Chem. Rev.* **2012**, *112*, 673; b) H.-C. Zhou, S. Kitagawa, *Chem. Soc. Rev.* **2014**, *43*, 5415; c) Q.-L. Zhu, Q. Xu, *Chem. Soc. Rev.* **2014**, *43*, 5468; d) Z. Zhang, M. J. Zaworotko, *Chem. Soc. Rev.* **2014**, *43*, 5444; e) T. Devic, C. Serre, *Chem. Soc. Rev.* **2014**, *43*, 6097; f) A. J. Howarth, Y. Liu, P. Li, Z. Li, T. C. Wang, J. T. Hupp, O. K. Farha, *Nat. Rev. Mater.* **2016**, *1*, 15018; g) Y. Fu, D. Sun, Y. Chen, R. Huang, Z. Ding, X. Fu, Z. Li, *Angew. Chem. Int. Ed.* **2012**, *51*, 3364.

[6] a) Y.-J. Tang, M.-R. Gao, C.-H. Liu, S.-L. Li, H.-L. Jiang, Y.-Q. Lan, M. Han, S.-H. Yu, *Angew. Chem. Int. Ed.* **2015**, *54*, 12928; b) J.-R. Li, J. Sculley, H.-C. Zhou, *Chem. Rev.* **2012**, *112*, 869; c) H.-L. Jiang, Q. Xu, *Chem. Commun.* **2011**, *47*, 3351; d) Z. Zhang, Z.-Z. Yao, S. Xiang, B. Chen, *Energy Environ. Sci.* **2014**, *7*, 2868; e) P.-Q. Liao, W.-X. Zhang, J.-P. Zhang, X.-M. Chen, *Nat. Commun.* **2015**, *6*, 8697; f) H.-Q. Xu, J. Hu, D. Wang, Z. Li, Q. Zhang, Y. Luo, S.-H. Yu, H.-L. Jiang, *J. Am. Chem. Soc.* **2015**, *137*, 13440; g) H.-X. Zhang, M. Liu, T. Wen, J. Zhang, *Coord. Chem. Rev.* **2016**, *307*, 255.

[7] a) B. Liu, H. Shioyama, T. Akita, Q. Xu, *J. Am. Chem. Soc.* **2008**, *130*, 5390; b) Y.-Z. Chen, C. Wang, Z.-Y. Wu, Y. Xiong, Q. Xu, S.-H. Yu, H.-L. Jiang, *Adv. Mater.* **2015**, *27*, 5010; c) Y.-X. Zhou, Y.-Z. Chen, L. Cao, J. Lu, H.-L. Jiang, *Chem. Commun.* **2015**, *51*, 8292; d) K. Shen, X. Chen, J. Chen, Y. Li, *ACS Catal.* **2016**, *6*, 5887; e) Y. V. Kaneti, J. Tang, R. R. Salunkhe, X. Jiang, A. Yu, K. C.-W. Wu, Y. Yamauchi, *Adv. Mater.* **2017**, *29*, 1604898; f) P. Zhang, F. Sun, Z. Xiang, Z. Shen, J. Yun, D. Cao, *Energy Environ. Sci.* **2014**, *7*, 442; g) D. Zhao, J.-L. Shui, L. R. Grabstanowicz, C. Chen, S. M. Commet, T. Xu, J. Lu, D.-J. Liu, *Adv. Mater.* **2014**, *26*, 1093; h) S. Zhao, H. Yin, L. Du, L. He, K. Zhao, L. Chang, G. Yin, H. Zhao, S. Liu, Z. Tang, *ACS Nano* **2014**, *8*, 12660; i) C. W. Abney, J. C. Gilhula, K. Lu, W. Lin, *Adv. Mater.* **2014**, *26*, 7993; j) C. W. Abney, K. M. L. Taylor-Pashow, S. R. Russell, Y. Chen, R. Samantaray,

J. V. Lockard, W. Lin, *Chem. Mater.* **2014**, *26*, 5231; k) L. Lux, K. Williams, S. Ma, *CrystEngComm* **2015**, *17*, 10; l) Q. Lin, X. Bu, A. Kong, C. Mao, X. Zhao, F. Bu, P. Feng, *J. Am. Chem. Soc.* **2015**, *137*, 2235; m) A. Mahmood, W. Guo, H. Tabassum, R. Zou, *Adv. Energy Mater.* **2016**, *6*, 1600423; n) K. J. Lee, S. Choi, S. Park, H. R. Moon, *Chem. Mater.* **2016**, *28*, 4403; o) M. Hu, J. Reboul, S. Furukawa, N. L. Torad, Q. Ji, P. Srinivasu, K. Ariga, S. Kitagawa, Y. Yamauchi, *J. Am. Chem. Soc.* **2012**, *134*, 2864; p) N. L. Torad, R. R. Salunkhe, Y. Li, H. Hamoudi, M. Imura, Y. Sakka, C.-C. Hu, Y. Yamauchi, *Chem. - Eur. J.* **2014**, *20*, 7895; q) J. Tang, Y. Yamauchi, *Nat. Chem.* **2016**, *8*, 638; r) R. R. Salunkhe, Y. V. Kaneti, J. Kim, J. H. Kim, Y. Yamauchi, *Acc. Chem. Res.* **2016**, *49*, 2796.

[8] X. Sun, Y. Shi, P. Zhang, C. Zheng, X. Zheng, F. Zhang, Y. Zhang, N. Guan, D. Zhao, G. D. Stucky, *J. Am. Chem. Soc.* **2011**, *133*, 14542.

[9] a) T. Loiseau, C. Serre, C. Huguenard, G. Fink, F. Taulelle, M. Henry, T. Bataille, G. Férey, *Chem. - Eur. J.* **2004**, *10*, 1373; b) I. Senkovska, F. Hoffmann, M. Fröba, J. Getzschmann, W. Böhlmann, S. Kaskel, *Microporous Mesoporous Mater.* **2009**, *122*, 93; c) K. S. Park, Z. Ni, A. P. Côté, J. Y. Choi, R. Huang, F. J. Uribe-Romo, H. K. Chae, M. O'Keeffe, O. M. Yaghi, *Proc. Natl. Acad. Sci. USA* **2006**, *103*, 10186; d) X.-C. Huang, Y.-Y. Lin, J.-P. Zhang, X.-M. Chen, *Angew. Chem. Int. Ed.* **2006**, *45*, 1557.

[10] a) P. Scherrer, *Göttingen Nachr. Math. Phys.* **1918**, *2*, 98; b) U. Holzwarth, N. Gibson, *Nat. Nanotechnol.* **2011**, *6*, 534; c) A. Monshi, M. R. Foroughi, M. R. Monshi, *World J. Nano Sci. Eng.* **2012**, *2*, 154.

[11] a) H. Yan, J. Yang, G. Ma, G. Wu, X. Zong, Z. Lei, J. Shi, C. Li, *J. Catal.* **2009**, *266*, 165; b) S. R. Lingampalli, U. K. Gautam, C. N. R. Rao, *Energy Environ. Sci.* **2013**, *6*, 3589.

[12] a) C. A. Kent, D. Liu, L. Ma, J. M. Papanikolas, T. J. Meyer, W. Lin, *J. Am. Chem. Soc.* **2011**, *133*, 12940; b) A. W. Peters, Z. Li, O. K. Farha, J. T. Hupp, *ACS Appl. Mater. Interfaces* **2016**, *8*, 20675.